

Measurements of the di-photon and photon + b jet differential production cross sections in $p\bar{p}$ collisions at $\sqrt{s} = 1.96$ TeV

Peter SVOISKY*[†]

University of Oklahoma

E-mail: psvoisky@gmail.com

We present measurements of the differential cross sections for the production of photon pairs and for the production of b jets in association with photons in $p\bar{p}$ collisions at $\sqrt{s} = 1.96$ TeV using data recorded with the DØ detector at the Fermilab Tevatron collider and corresponding to an integrated luminosity of 4.2 fb^{-1} and 8.7 fb^{-1} , respectively. Results are compared with the prediction of NLO QCD calculations and with the predictions of Monte Carlo event generators.

*36th International Conference on High Energy Physics,
July 4-11, 2012
Melbourne, Australia*

*Speaker.

[†]For the DØ Collaboration

1. Introduction

High-energy photons (γ) coming from a hard hadron-hadron scattering are ideal probes of parton level dynamics. Events where such photons are produced in association with a b quark are a valuable source of information about the b quark and gluon (g) parton distribution functions (PDFs) of the incoming hadrons. Di-photon events are excellent material for new phenomena searches, such as new heavy resonances [1], extra spatial dimensions [2], and cascade decays of new heavy particles [3], not mentioning the recent discovery of a new boson by the LHC experiments [4, 5]. Photons are indispensable for such studies because of their higher detector resolution in comparison to hadronic jets.

At the Tevatron the leading process contributing to $\gamma + b$ jet production is b quark gluon scattering, $gb \rightarrow \gamma b$, see Fig. 1, but at photon transverse momenta (p_T^γ) of ≈ 70 GeV quark-antiquark annihilation $q\bar{q} \rightarrow \gamma b\bar{b}$ starts dominating. The $b\bar{b}$ pair is the result of a gluon splitting [6]. A high-energy photon can also be produced in close proximity to a hadronic jet as a result of a non-perturbative process of parton fragmentation, such as in $gg \rightarrow b\bar{b}$ or $gb \rightarrow gb$. However, in such cases, it is poorly isolated from the hadronic activity and loses its high resolution advantage. The contribution of such photons can be suppressed by using strong isolation requirements.

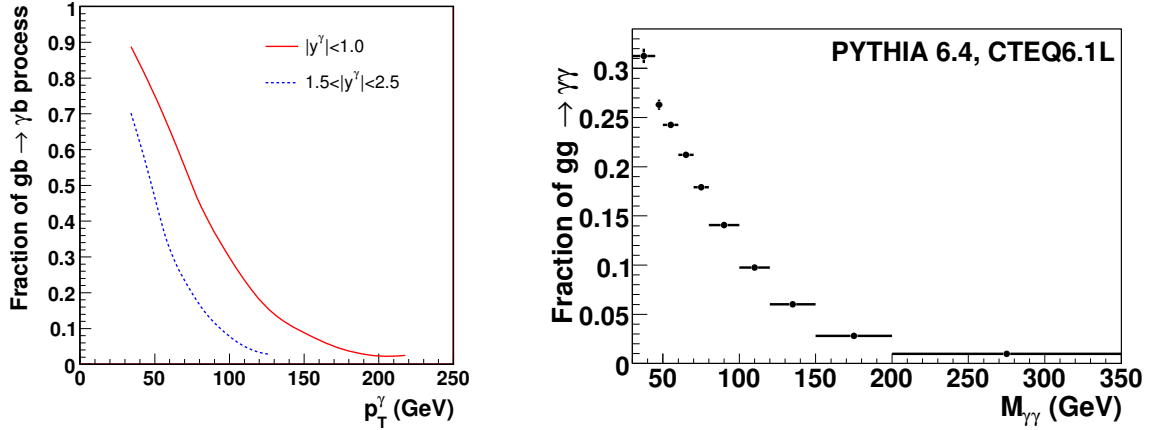


Figure 1: Fraction of events produced in the "Compton-like" scattering $gb \rightarrow \gamma b$ subprocess of the associated production of direct photon and a b jet as a function of p_T^γ (left) [9], and fractional contribution of the gluon fusion $gg \rightarrow \gamma\gamma$ subprocess in the direct photon pair production as a function of the pair invariant mass $M_{\gamma\gamma}$ (right) [10].

In addition to new phenomena searches, high-energy di-photon events are a useful tool to test the validity of the predictions of perturbative quantum chromodynamics (pQCD) and soft-gluon resummation methods featured in theoretical calculations [7]. Direct photon pairs (DPP) [8] are predominantly produced at the Tevatron through the quark-antiquark scattering ($q\bar{q} \rightarrow \gamma\gamma$), however at low DPP masses the higher gg parton luminosity is responsible for a significant contribution from gluon-gluon fusion ($gg \rightarrow \gamma\gamma$) despite an additional suppression factor of α_s^2 , see Fig. 1. In DPP events, as in $\gamma + b$ jet production, one or both photons can be produced in parton fragmentation processes [7, 8]. Their contribution can be reduced using tight constraints on the photon isolation.

2. Measurements

We describe measurements of the inclusive differential cross sections of $\gamma + b$ jet production as a function of the p_T^γ and DPP production as functions of the pair mass $M_{\gamma\gamma}$, pair transverse momentum $p_T^{\gamma\gamma}$, azimuthal angle between the photons $\Delta\phi_{\gamma\gamma}$, and the polar scattering angle of the photon pair in the Collins-Soper frame $\cos\theta^*$ [11]. For the first time, double differential cross sections are measured for the DPP production. The $\gamma + b$ jet measurement uses a dataset collected with the D0 detector at the Fermilab Tevatron between June 2006 and September 2011, while the dataset for the DPP measurement uses a smaller part of it collected between August 2006 and June 2009.

The D0 detector is a general purpose detector described in detail elsewhere [12]. The sub-detectors most relevant for the photon-jet analyses are the tracking system with the silicon micro-strip tracker (SMT), central fiber tracker (CFT), both embedded in a 2 T solenoidal magnetic field, central preshower detector (CPS), located right outside the magnet, and the three-cryostat liquid-argon calorimeter. The central section of the calorimeter covers the region $|\eta_{det}| < 1.1$, where η_{det} is the pseudorapidity with respect to the geometric center of the D0 detector, while the two end calorimeters cover the region up to $|\eta_{det}| \approx 4.2$. The four inner layers of the calorimeter constitute the electro-magnetic (EM) section and are segmented into cells with 0.1×0.1 size in $\Delta\phi \times \Delta\eta$, except for the third layer, where the granularity is 0.05×0.05 . It allows a precise measurement of the photon energy with 3.6% resolution at 50 GeV and direction measurement with 0.01 radian resolution. The energy response of the calorimeter is calibrated using electrons from Z boson decays. Corrections for the difference between the calorimeter response of photons and electrons amount to 2% and are obtained from a detailed GEANT-based [14] Monte Carlo (MC) simulation of the D0 detector using the same software reconstruction as in data. The MC events are overlaid with events from random $p\bar{p}$ crossings with a similar instantaneous luminosity spectrum as in data to accurately model the effects of multiple $p\bar{p}$ interactions and detector noise.

The $\gamma + b$ jet dataset and the DPP dataset correspond to 8.7 fb^{-1} and 4.2 fb^{-1} of integrated luminosity, respectively. Data for the $\gamma + b$ jet cross section measurement are collected using a set of triggers requiring at least one, and for the DPP, at least two clusters of energy in the electromagnetic calorimeter with loose shower shape requirements. The trigger efficiency is $\geq 96\%$ for the photon candidate selection in both cases.

The $\gamma + b$ jet production cross sections are measured in the central $|y^\gamma| < 1.0$ and forward $1.5 < |y^\gamma| < 2.5$ photon rapidity regions. Rapidity is calculated as a function of the polar angle θ between the particle flight direction and the proton beam axis as $y = \frac{1}{2} \ln[(1 + \beta \cos\theta)/(1 - \beta \cos\theta)]$, where β is the particle velocity relative to the speed of light $\beta = |\vec{p}|/E$. Photons are required to have $30 < p_T^\gamma < 300$ GeV in the central and $30 < p_T^\gamma < 200$ GeV in the forward regions. The analysis selection requires the b jet absolute rapidity to be constrained by $|y^{jet}| < 1.5$ and the transverse momentum by $p_T^{jet} > 15$ GeV. Such selection allows to cover parton momentum fractions within the range $0.007 \lesssim x \lesssim 0.4$ [9].

For DPP, along with the sensitivity of $M_{\gamma\gamma}$ to beyond the Standard Model phenomena, $p_T^{\gamma\gamma}$ and $\Delta\phi_{\gamma\gamma}$ distributions reveal the effects of initial state gluon radiation and parton fragmentation. In their turn, the PDFs and the final state angular momentum affect the shape of $\cos\theta^*$, approximated in the analysis as $\cos\theta^* \approx \tanh[(\eta_1 - \eta_2)/2]$, allowing to distinguish between the DPP background and,

for example, a spin-0 Higgs boson [10, 13]. $\eta_{1,2}$ are pseudorapidities of the photons equal to their rapidities due to their masslessness. Both photons are required to be in the central region $|\eta| < 0.9$, be separated by an angular distance $\Delta R = \sqrt{(\Delta\phi)^2 + (\Delta\eta)^2} > 0.4$, and pass uneven transverse momentum cuts $p_T^\gamma > 21(20)$ GeV for the leading (sub-leading) photons to avoid divergencies in the NLO theoretical calculations, described in [7, 8].

These analyses share the same photon reconstruction algorithm and photon quality cuts. Photons are reconstructed as clusters of projective towers of calorimeter cells with high energy deposits inside a cone of radius $R = 0.4$. The cluster energy is calculated by summing up energies of projective towers inside a smaller cone of radius $R = 0.2$. Photon candidates are selected by requiring: (i) the fraction of the energy deposited into the EM layers of the calorimeter to be $> 97\%$; calorimeter isolation $I = [E_{tot}(0.4) - E_{EM}(0.2)]/E_{EM}(0.2) < 0.07$, where $E_{tot}(R)[E_{EM}(R)]$ is the total [EM only] energy in a cone of radius R ; (iii) scalar sum of the p_T of the tracks originating from a primary $p\bar{p}$ interaction point in an annulus $0.05 < R < 0.4$ around its axis, calculated from the tracks with $p_T > 0.5$ GeV, to be < 1.5 GeV; (iv) energy weighted sum of the EM cell energies to be consistent with the EM shower. The large electron background is suppressed by applying an anti-track match selection, which is the absence of a reconstructed track matched to the EM cluster or, in the central pseudorapidity region, significant tracker activity in the SMT or CFT, consistent with an electron track.

Further suppression of jets as a background to the photon candidates is done via an artificial neural network discriminant (γ -NN) trained on PYTHIA [15] MC samples of photon and jet production. γ -NN relies on the differences in the tracker activity, energy deposits in the calorimeter, and in the CPS in the central rapidity region. The γ -NN output distributions for photons are in good agreement between data and MC and provide significant separation between photons and jets [9, 10]. The photon candidates in both analyses are required to have an γ -NN output > 0.3 . This selection is $\approx 98\%$ efficient for photons.

The $\gamma + b$ jet measurement uses the D0 Run II algorithm [16] with a cone size $R = 0.5$ to reconstruct hadronic jets. In addition to the kinematic cuts mentioned above jets are required to have at least two associated tracks with $p_T > 0.5$ GeV with at least one hit in the SMT each, and the highest p_T of the tracks to be > 1.0 GeV. The jets that pass these quality cuts are subjected to a selection based on the b jet identification neural net discriminant (b -NN), which is (40 – 52)% efficient for b jets, depending on the accompanying photon p_T bin. The b -NN uses several variables emphasizing the property of a heavy-flavor jet to have displaced (secondary) vertices inside it due to decays of short-lived heavy-flavor hadrons [17]. One of such variables, the invariant mass of the charged particle tracks associated with the secondary vertex (M_{SV}) is used to determine fractions of the b quark jets, c quark jets, and light flavor jets in data by fitting jet templates to data [9]. The estimated fraction of b jets grows with p_T^γ from 35% to 42%.

To calculate the cross sections, the fraction of background events is estimated among the candidate events in data. In $\gamma + b$ jet measurement, an additional background of multi-jet events, where a jet can be misidentified as a photon, is estimated by fitting templates of the γ -NN distributions for photons and jets to the γ -NN distribution in data for each p_T^γ bin. The observed photon purities range from 62% to 99% in the central rapidity and from 40% and 55% in the forward rapidity regions. The amount of multijet background in the DPP measurement is calculated with the help of a 4×4 matrix method using numbers of candidate events in data and efficiencies of passing two

different cuts on the γ -NN in simulation. The average purity of the DPP candidates in data is found to be $\approx 67\%$ [10]. Additional backgrounds from $Z(\rightarrow e^+e^-)+\text{jet}$ and $W(\rightarrow e\nu)+\text{jet}$ events are estimated from simulation and found to be $\lesssim 1\%$ in $\gamma+b$ jet and $\approx 1.6\%$ in DPP analyses.

In both measurements results are presented at particle level, considering all stable particles as defined in Ref. [18]. In order to do this, the observed numbers of candidate events are corrected for the efficiency of the selection of both a photon and a jet in the $\gamma+b$ jet case, and two photons in the DPP case, and also for the detector acceptance of such selection. For the $\gamma+b$ jet measurement this is done using events simulated with SHERPA [19] and PYTHIA event generators, processed through a GEANT-based D0 detector simulation and the same reconstruction algorithms as in the data. For the DPP analysis the efficiency is measured in events generated by PYTHIA and processed through the full event simulation and reconstruction as above, while the detector acceptance is measured in event samples generated by RESBOS [7] event generator and processed through a fast simulation using data driven efficiencies and parameters to increase the MC statistics. In the $\gamma+b$ jet analysis case photon acceptance varies between $(82-90)\%$ and jet acceptance between $(88-100)\%$, while the efficiency of the photon selection is $(68-85)\%$. The DPP detector acceptance varies between $(45-64)\%$, while the DPP selection efficiency is $\approx 64\%$.

3. Results

The cross section results are compared to next-to-leading (NLO) order pQCD predictions with the renormalization μ_R , factorization μ_F , and fragmentation μ_f scales set to p_T^γ in the $\gamma+b$ jet case and to $M_{\gamma\gamma}$ in the DPP case. In all of the theoretical predictions the photon isolation is set to $E_T^{\text{iso}} = E_T^{\text{tot}}(0.4) - E_T^\gamma < 2.5$ GeV, where $E_T^{\text{tot}}(0.4)$ is the transverse energy within a cone of radius $R=0.4$, and E_T^γ is the photon transverse energy. Fig. 2 shows the ratio of the measured differential $\gamma+b$ cross section and NLO predictions as a function of the p_T^γ in the central rapidity region (left). The best agreement is obtained with the prediction from the SHERPA event generator, allowing for two hard partons (jets) in addition to the photon and b -quark in the final state. NLO QCD predictions show the need for higher order perturbative corrections and resummation of diagrams with additional gluon radiation in the region above $p_T^\gamma \gtrsim 70$ GeV. Fig. 2 also shows the differential DPP production cross section $d\sigma/dM_{\gamma\gamma}$ compared to the NLO predictions from SHERPA, RESBOS, DIPHOX, and PYTHIA event generators (right), where the prediction from SHERPA event generator again shows the best agreement with data. All theoretical predictions use CTEQ6.6M PDF set [20], except for the PYTHIA prediction with tune "A" in the DPP case, which uses CTEQ5L PDF set.

References

- [1] S. Mrenna and J. Wells, Phys. Rev. D **63**, 015006 (2001), and references therein.
- [2] M. C. Kumar, P. Mathews, V. Ravindran, and A. Tripathi, Phys. Lett. B **672**, 45 (2009).
- [3] G. F. Giudice and R. Rattazzi, Phys. Rep. **322**, 419 (1999).
- [4] G. Aad *et al.* (ATLAS Collaboration), Phys. Lett. B **716**, 1 (2012).
- [5] S. Chatrchyan *et al.* (CMS Collaboration), Phys. Lett. B **716**, 30 (2012).
- [6] T. Stavreva and J. F. Owens, Phys. Rev. D **79**, 054017 (2009).

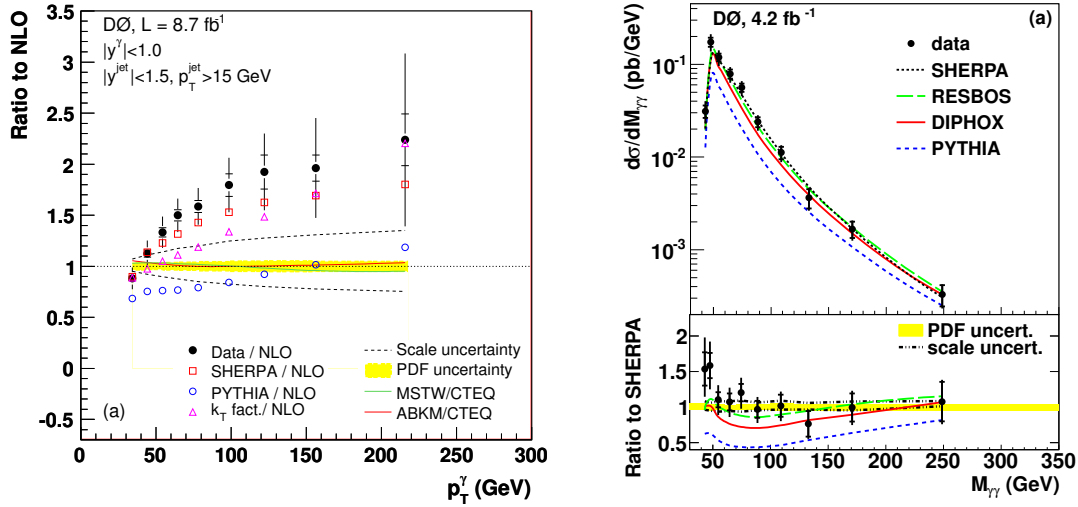


Figure 2: Ratio of the differential cross section of the associated production of a direct photon and a b-jet to the NLO QCD predictions as a function of p_T^γ (left) [9], and the differential cross section of the direct photon pair production as a function of the pair invariant mass $d\sigma/dM_{\gamma\gamma}$ and ratio to pQCD predictions (right) [10].

- [7] C. Balazs, E. L. Berger, P. Nadolsky, and C.-P. Yuan, Phys. Rev. D **76**, 013009 (2007).
- [8] T. Binoth, J.-Ph. Guillet, E. Pilon, and M. Werlen, Eur. Phys. J. C **16**, 311 (2000).
- [9] V. M. Abazov *et al.* (D0 Collaboration), Phys. Lett. B **714**, 32 (2012).
- [10] V. M. Abazov *et al.* (D0 Collaboration), Phys. Lett. B **690**, 108 (2010).
- [11] J. C. Collins, D. E. Soper, Phys. Rev. D **16**, 2219 (1977).
- [12] V. M. Abazov *et al.* (D0 Collaboration), Nucl. Instrum. Methods in Phys. Res. A **565**, 463 (2006); M. Abolins *et al.*, Nucl. Instrum. Methods in Phys. Res. A **584**, 75 (2007); R. Angstadt *et al.*, Nucl. Instrum. Methods in Phys. Res. A **622**, 298 (2010).
- [13] C. Balazs, E. L. Berger, S. Mrenna, and C.-P. Yuan, Phys. Rev. D **57**, 6934 (1998).
- [14] R. Brun and F. Carminati, CERN Program Library Long Writeup, W5013, (1993); we use GEANT version v3.21.
- [15] T. Sjostrand, S. Mrenna, and P. Z. Skands, J. High Energy Phys. **05**, 026 (2006). We use pythia version v6.420 with tune A.
- [16] G. C. Blazey *et al.*, arXiv:hep-ex/0005012 (2000).
- [17] V. M. Abazov *et al.* (D0 Collaboration), Nucl. Instrum. Methods in Phys. Res. A **620**, 490 (2010).
- [18] C. Buttar *et al.*, arXiv:0803.0678 [hep-ph], section 9.
- [19] T. Gleisberg *et al.*, J. High Energy Phys. **02**, 007 (2009). We use sherpa version v1.3.1.
- [20] W. K. Tung *et al.*, J. High Energy Phys. **02**, 053 (2007).